THE ROYAL SOCIETY

Nonlinear analyses of roll motion of a flooded ship in waves

By S. Murashige[1], T. Yamada[2] and K. Aihara[1,3]

[1]*Department of Mathematical Engineering and Information Physics, School of Engineering, The University of Tokyo, 7-3-1 Hongo, Bunkyo-ku, Tokyo 113-8656, Japan*

[2]*AIHARA Electrical Engineering Co. Ltd, 2-16-8 Hamacho, Funabashi, Chiba 273-0012, Japan*

[3]*CREST, Japan Science and Technology Corporation (JST), 4-1-8 Hon-cho, Kawaguchi, Saitama 332, Japan*

This paper investigates nonlinear responses of a flooded ship in regular waves. In previous experimental work, we found that the roll motion of a flooded ship can exhibit complicated irregular behaviour even in waves of a moderate height. First, we analyse the fractal dimension and the Lyapunov exponents of the experimental data and show that they have chaotic characteristics. We also show that a radial basis function network obtained directly from the data can reproduce a geometrical structure of the reconstructed attractor and provide good short-term prediction on the dynamical motion. Next, in order to understand this nonlinear phenomenon, we derive a simple mathematical model for the nonlinearly coupled motion of roll and flooded water in regular waves. This model has a form of coupled Duffing's equations with a bistable restoring term and a nonlinear inertial coefficient matrix. We obtain bifurcation diagrams of periodic solutions of this model and examine the intricate structure of this nonlinear system. Chaotic responses are found in wide regions of the parameter space, even if the wave-exciting moment is not large. Furthermore, the attractor structure of the chaotic solution is similar to that of the measured chaotic motion in the experiments. The results suggest that bifurcation analyses in this work help us understand the complex dynamics of nonlinear motion of a flooded ship in waves.

Keywords: nonlinear roll motion; flooded ship; bifurcation; chaos; nonlinear time-series analysis; coupled Duffing's equations

1. Introduction

A ship in waves can exhibit nonlinear responses which may lead to undesirable motion, including capsizing. Thus this problem has been one of the important subjects in the field of naval architecture. We can regard ship motion in regular waves as motion of a rigid body with periodic forcing. In general, a restoring moment of a ship in the direction of roll is nonlinear with respect to the roll angle ϕ, and the nonlinearity can cause complex roll responses in waves. This paper focuses on nonlinear roll motion of a flooded ship in waves. It is well known that flooded water has some critical effects on ship motion in waves, but dynamical stability of a flooded

ship in waves has not been made clear yet. In previous work (Murashige & Aihara 1998*a*,*b*; Murashige *et al*. 1999), we indicated the possibility that nonlinearly coupled dynamics of roll and flooded water is the key to understanding this problem.

A lot of nonlinearly coupled systems exist in the wide range of science and engineering fields; for example, mechanical vibrations (Nayfeh & Mook 1979; Moon 1992), fluid motion (Miles & Henderson 1990), electrical circuits (Yoshinaga & Kawakami 1989), neural systems (Skarda & Freeman 1987), and so on. It is not easy to elucidate the intricate mechanism of these systems, but application of the dynamical system theory is one of a number of promising approaches. The basic idea of this approach is to qualitatively catch essential features of dynamical systems in a state space. Nonlinear dynamical systems with periodic forcing can show various types of phenomena; for example, coexistence of several periodic responses which are correlated with jump and hysteresis behaviours, nonlinear resonances, quasi-periodic responses, chaotic responses, etc. Qualitative change of a phase portrait with variation of values of system parameters in a dynamical system is referred to as a bifurcation. Thus bifurcation analyses are required as a first step of nonlinear system analyses. The codimension-one bifurcations of periodic responses are classified into three types: the saddle-node, the period-doubling and the Neimark–Sacker bifurcations, which correspond to generation of a pair of stable and unstable periodic responses, branching of a periodic response with a doubled period, and appearance of a quasi-periodic response, respectively. Kawakami (1984) presented the numerical method to obtain a set of the codimension-one bifurcations. This method can also be applied to the codimension-two bifurcations which, in general, occur under coexistence of two different kinds of bifurcation conditions. Yoshinaga & Kawakami (1989) pointed out that the codimension-two bifurcation is deeply related to generation of chaotic responses in a coupled system.

Many researchers have considered nonlinear ship motion in waves (for example, Paulling & Rosenberg 1959; Nayfeh *et al*. 1973; Wright & Marshfield 1980; Virgin 1987; Nayfeh 1988; Kan & Taguchi 1990; Rainey & Thompson 1991; Soliman & Thompson 1991; Thompson *et al*. 1992; MacMaster & Thompson 1994). Thompson gave a comprehensive review in this field (Thompson 1997). There are also some works on motion of a flooded ship in waves (Dillingham 1981; Falzarano *et al*. 1992; Thompson & de Souza 1996). Some of these works investigated this problem from the viewpoint of nonlinear dynamics, using mathematical models for ship motion in waves. On the other hand, we consider that not only theoretical, but also experimental, works are indispensable, because it is hard to get an exact mathematical model for this complex problem. In addition, since the conventional linear time-series analyses are not suitable for chaotic data, experimental works require careful treatments for nonlinear time-series.

We performed experiments using a ferry model (the length between perpendiculars was 4.3 m, with a scale ratio of 1:23.5) in a wave tank of 8 m wide, 50 m long and 4.5 m deep, and measured the roll angle ϕ of a flooded ship in regular beam waves (Murashige & Aihara 1998*b*). Then it was found that a coupled system of roll and flooded water in waves can exhibit nonlinear responses even in waves of a relatively moderate height. For example, two completely different motions coexist under the same wave conditions, and the reconstructed attractor of one of them looked like a chaotic one. In addition, in order to examine this system in more detail, we conducted some simplified two-dimensional experiments using a box-shaped model (scale ratio

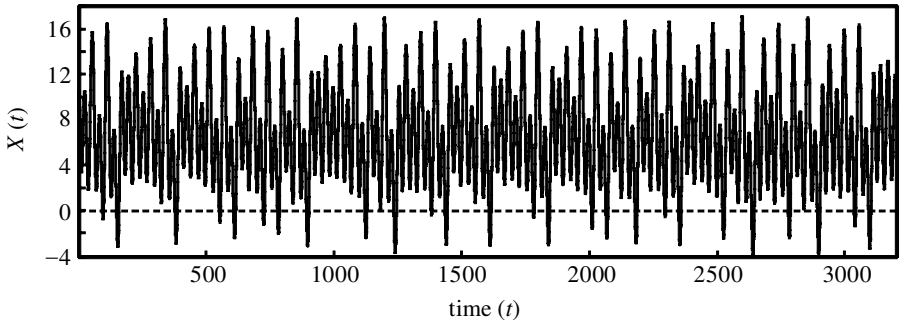

Figure 1. Time-series data of the measured roll angle $\phi(t)$ in the experiment with the box-shaped model ($X(t)$=$\phi(t)$, X measured in degrees).

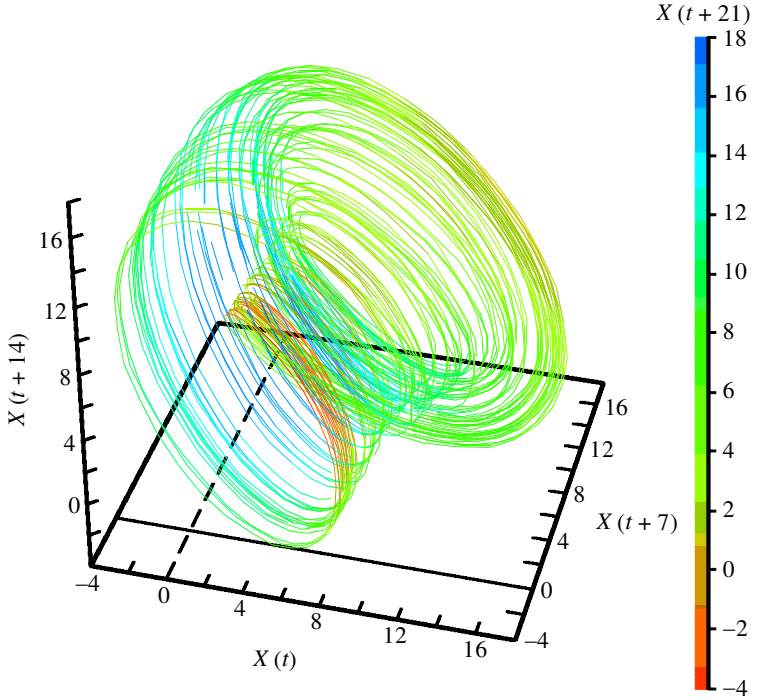

Figure 2. Phase portrait of a possible attractor reconstructed from the experimental data of the box-shaped model. The values of the reconstruction dimension and the lag are 4 and 7, respectively ($(X(t), X(t+\tau), X(t+2\tau)) = (\phi(t), \phi(t+\tau), \phi(t+2\tau))$, X measured in degrees).

of 1:35.6) in the same wave tank as the ferry model, and measured the roll angle in regular waves. This model without flooded water showed only regular motion with the same period as the waves, but the flooded model demonstrated complicated bifurcation phenomena. The irregular motion found in the experiments was chaotic in the sense that the stroboscopic plots show the stretching, folding and compressing process, and that the maximum Lyapunov exponent is positive. It should be noted that chaotic motion was found in wide regions of a parameter space. From observations of these experiments, we conjectured that coupling of roll and flooded water

is dominant in this system, and that free surface motion of flooded water might not be critical. These results lead to some assumptions for the mathematical model of this problem (Murashige *et al.* 1999). In this model, we assumed that the surface of flooded water is flat but not horizontal, and that motion of flooded water can be represented by the inclination of the surface χ. Then the mathematical model was expressed as ordinary differential equations with respect to the roll angle ϕ and χ. We numerically obtained some bifurcation sets of periodic solutions of this model, and considered the relation between bifurcation and nonlinear resonances. The results qualitatively agreed with the experimental results.

This paper shows nonlinear time-series analyses of the experimental data in more detail than previous work (Murashige & Aihara 1998*b*), and bifurcation analyses using a simplified mathematical model to investigate the generation of chaotic responses found in the experiments. Section 2 shows the fractal dimension and the Lyapunov exponents of the experimental data, and demonstrates nonlinear modelling and prediction of the chaotic response by the radial basis function (RBF) network. Section 3 shows some characteristics of the nonlinearly coupled system of roll and flooded water in waves, and derives a new mathematical model for such complex forced chaos. Section 4 represents some results of bifurcation analyses using this model, and discusses chaotic responses. Finally, § 5 concludes this paper.

2. Nonlinear time-series analyses of the experimental data

In this section, we analyse experimental data observed from a box-shaped model (Murashige & Aihara 1998*b*), from a viewpoint of nonlinear time-series analyses (Parker & Chua 1989; Ott *et al.* 1994; Abarbanel 1996; Kantz & Schreiber 1997). In the nonlinear time-series analyses, techniques such as estimation of the fractal dimension and the Lyapunov spectrum and time-series forecasting with deterministic nonlinear modelling are widely used to characterize the nonlinear dynamics of a system and detect possible deterministic chaos only from observed data, without any *a priori* knowledge of the system. Although all state variables of a nonlinear system cannot usually be observed and one can often obtain just only one set of scalar time-series data, embedding theory (Takens 1981; Sauer *et al.* 1991) guarantees that a single time-series is generic or prevalent enough to reconstruct an attractor of the objective system if the reconstruction dimension with delay coordinates is large enough. In this section, we analyse time-series data on roll motion of the box-shaped model in order to elucidate underlying possibly chaotic dynamics. In particular, we calculate the correlation dimension and the Lyapunov spectrum of the measured time-series data, and construct a nonlinear deterministic model from which the free-run attractor can reproduce the geometrical structure of the reconstructed attractor. These results suggest that the experimental data of the box-shaped model are chaotic, probably caused by the nonlinear dynamics of the flooded ship in waves.

(*a*) *Methods of nonlinear time-series analyses*

To estimate the fractal dimension, the Grassberger–Procaccia method with correlation function (Grassberger & Procaccia 1983*a*,*b*) has been widely used in the past, but it is now well known that this method has some subtle problems (Parker & Chua 1989; Ruelle 1990; Abarbanel 1996; Kantz & Schreiber 1997). Thus we adopt

an improved dimension estimator proposed by Judd (1992, 1994). In this method, it is assumed that a local structure of a strange attractor can be generally modelled as a Cartesian product of a Cantor-like set and a bounded and connected subset of a smooth manifold. Under this assumption, the correlation dimension is estimated on the basis of the maximum-likelihood method with a change in the cut-off value r_0 marking the scale at which relevant scaling information on the dimension begins (Judd 1992).

The Lyapunov spectrum composed of the Lyapunov exponents is an important indicator in characterizing deterministic chaos in relation to orbital instability. Eckmann & Ruelle (1985) and Sano & Sawada (1985) proposed a method to estimate Jacobian matrices from the time-series data. Here we adopt this method and combine it with a numerical procedure by Shimada & Nagashima (1979) to estimate the Lyapunov spectrum $\{\lambda_1, \lambda_2, \ldots, \lambda_k; \lambda_i \geqslant \lambda_{i+1}, k \text{ is the reconstruction dimension}\}$ from the observed time-series data. In addition, we can obtain the Lyapunov dimension D_{L} defined by

$$D_{\mathrm{L}} = j + \sum_{i=1}^{j} \lambda_i / |\lambda_{j+1}|,$$

where j is the largest integer such that

$$\sum_{i=1}^{j} \lambda_i \geqslant 0.$$

If we can predict the short-term future of a system with a deterministic model, it implies that the system behaves according to such deterministic dynamics, even though its behaviour appears to be very erratic (Farmer & Sidorowich 1987; Casdagli 1989; Sugihara & May 1990). We use the RBF network (Casdagli 1989; Smith 1993) as the nonlinear modelling method approximating the dynamics underlying the time-series data. Here we adopt the Gaussian function $g(x) = \exp(-Bx^2)$, with the coefficient B as the radial basis function and the smoothing-RBI (radial basis interpolation) method (Suzuki *et al.* 1993), which is available for noisy data by adjusting a trade-off parameter between fitting accuracy and smoothness.

(*b*) *Results of nonlinear time-series analyses*

In this subsection, we analyse the experimental data of the box-shaped model shown in figure 1. In the analysis, we use delay coordinates

$$\boldsymbol{X}(t) = X(t), X(t+\tau), \ldots, X(t+(n-1)\tau)$$

of the time-series data $\{X(t)\}$ with the reconstruction dimension n and the lag τ, where the discrete-time series of $\{X(t)\}$ corresponds to that of the roll angle $\phi(t)$ measured from the box-shaped model with the sampling time of 0.05 s. Figure 2 demonstrates a reconstructed attractor with $n = 4$ and $\tau = 7$, where $\tau = 7$ corresponds to 0.05×7 s.

Figure 3 shows estimated dimensions of the experimental data reconstructed with $n = 3$, 4, 5, 7, 10 and 14, and $\tau = 7$. The result shows that the estimated correlation dimension is between 2.24 and 2.27 at relevant small cut-off values.

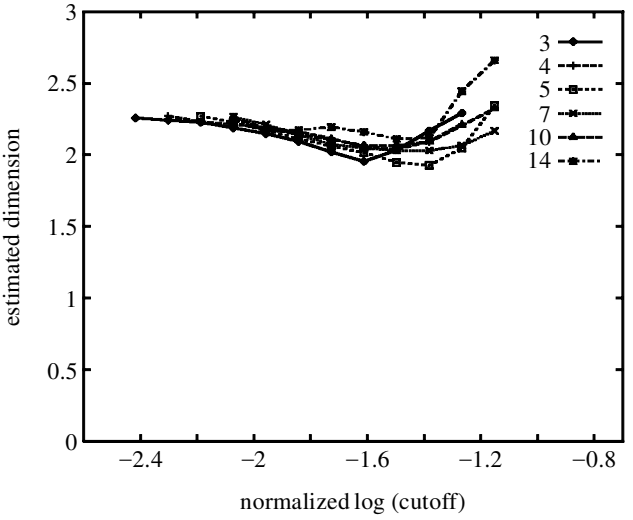

Figure 3. Estimated dimensions of the experimental data reconstructed with $n = 3$, 4, 5, 7, 10 and 14, and $\tau = 7$.

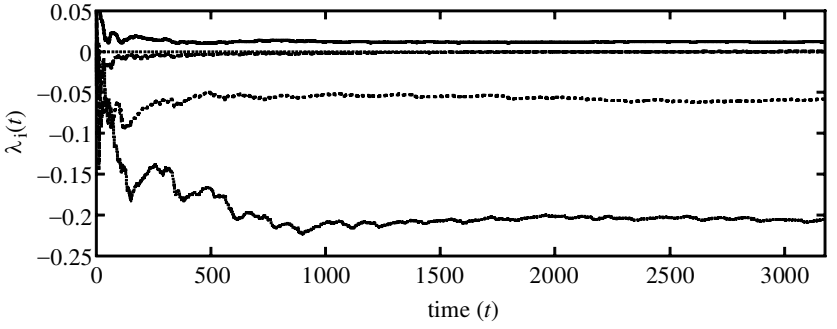

Figure 4. The estimated Lyapunov spectrum of the experimental data reconstructed with $n = 4$ and $\tau = 7$. The number of neighbours to be used for estimation of the Jacobian matrices is 35. The converged values of Lyapunov exponents are 0.0118, 0.000 378, −0.0580 and −0.205. The estimated Lyapunov dimension is 2.20.

Figure 4 shows the estimated Lyapunov spectrum of the data reconstructed with $n = 4$ and $\tau = 7$. The result shows that the experimental data have a positive largest Lyapunov exponent and the Lyapunov dimension D_{L} is estimated to be about 2.20. In addition, other calculations with 20 to 70 neighbours provide the similar positive Lyapunov exponents and the Lyapunov dimension between 2.2 and 2.3.

Figure 5 shows a free-run attractor of the nonlinear model of the RBF network model derived from the experimental data reconstructed with $n = 4$ and $\tau = 7$. The result shows that the attractor obtained by making the dynamical system of the RBF network run freely from the initial condition corresponding to the last state of the input dataset is quite similar to the original reconstructed attractor shown in figure 2. Figure 6 shows the relative root mean square error (RRMSE) of the prediction calculated by the RBF network. The result suggests that this RBF model is an appropriate predictor for forecasting the behaviour of the system in

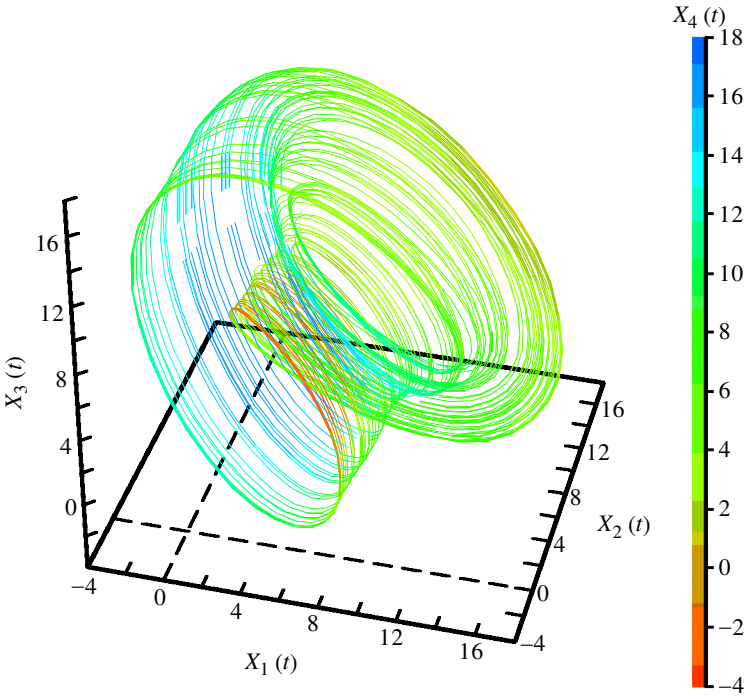

Figure 5. A free-run attractor of a nonlinear model of the RBF network derived from the experimental data reconstructed with $n = 4$ and $\tau = 7$. The number of training data is 1000. The number of iterations of free running is 3000. The number of bases for the RBF network is 200. We set the value of the trade-off parameter to be 0.01 (X measured in degrees).

the short-term future of about 200 steps, and the prediction error shows a chaotic characteristic with short-term predictability and long-term unpredictability based upon the deterministic model. Figure 7 shows the Lyapunov spectrum calculated with the Jacobian matrix of the RBF network. This result shows that the free-run attractor is chaotic, with a positive largest Lyapunov exponent similar to that of figure 4. The Lyapunov dimension of 2.16 is also satisfactorily close both to the estimated Lyapunov dimension of 2.20 in figure 4 and to the estimated correlation dimensions of 2.24–2.27 in figure 3.

All the results of the nonlinear time-series analyses suggest that the experimental data of the box-shaped model are typically chaotic; this is possibly caused by the underlying nonlinear dynamics of the system of the flooded ship forced by waves.

3. Mathematical model

In a previous paper (Murashige *et al.* 1999), we derived a mathematical model for nonlinearly coupled motion of roll and flooded water in regular waves. This model produced nonlinear roll responses which qualitatively agreed with the experimental results. But we had some difficulties for bifurcation analyses due to artificially introduced assumptions in the model. This section summarizes the basic ideas to derive the original mathematical model in § 3 *a* and derives a new model in § 3 *b*

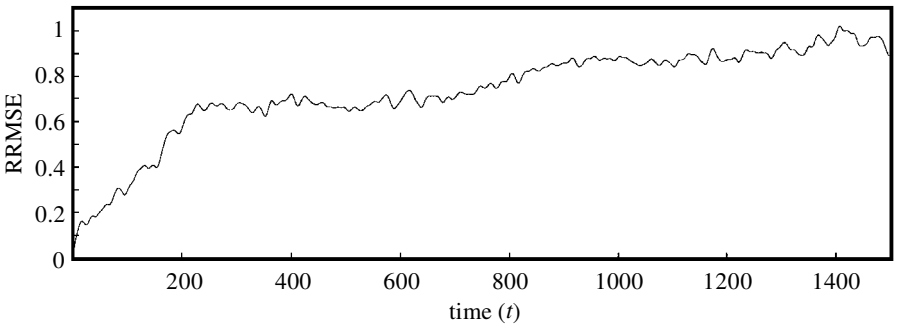

Figure 6. The relative root mean square error (RRMSE) of the prediction by the RBF network with the same condition as in figure 5.

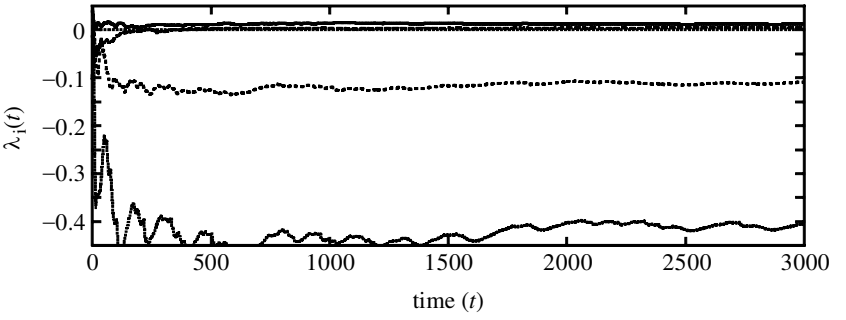

Figure 7. The Lyapunov spectrum of the nonlinear model. The converged values of the Lyapunov exponents are 0.0123, 0.004 85, −0.109 and −0.405. The calculated Lyapunov dimension is 2.16.

which maintains the essential properties of the original model but is more suitable for bifurcation analyses.

(*a*) *Modelling of nonlinearly coupled motion of ship roll and flooded water in waves*

In order to investigate the nonlinear phenomena found in the experiments, we consider the two-dimensional motion of a box-shaped ship with flooded water in the vertical cross-section parallel to the progressing direction of regular waves, as shown in figure 8. In previous work (Murashige *et al.* 1999), we obtained a mathematical model for the coupled motion of roll and flooded water in regular waves, based on the following five assumptions.

(i) Coupling of roll motion and flooded water is dominant, and sway and heave modes can be neglected.

(ii) The surface of flooded water is flat with slope χ (or θ).

(iii) The motion of flooded water can be approximated by that of a material particle located at the centre of gravity G_{w}.

(iv) The wave-forcing moment varies sinusoidally with the same angular frequency Ω as the incident waves.

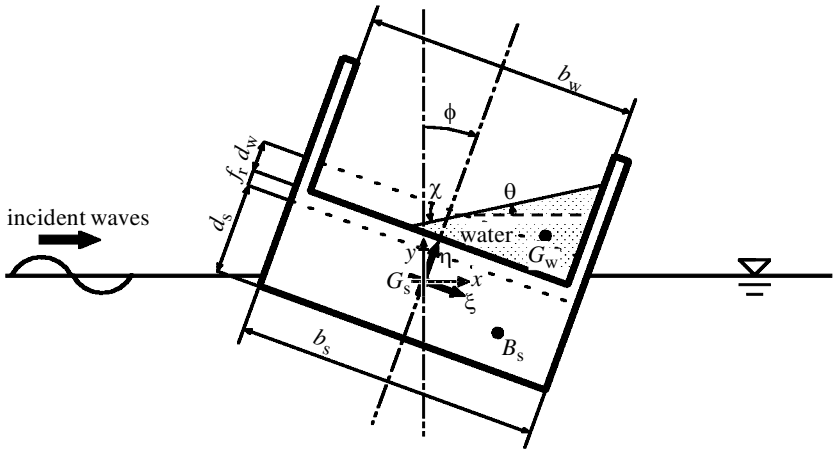

Figure 8. Illustration of the simplified motion of a flooded ship in waves. Here, ϕ denotes the roll angle of a ship, χ the slope of the surface of flooded water, b_s the breadth of a ship, b_w the breadth of an inside area of a ship, d_s the draft, f_r the freeboard, d_w the depth of flooded water, G_s the centre of gravity of a ship, G_w the centre of gravity of flooded water, and B_s the centre of buoyancy of a ship.

(v) The damping moments on the ship and the flooded water vary linearly with $\dot{\phi}$ and $\dot{\chi}$ (where the dot denotes differentiation with respect to t), respectively.

In this model, the kinetic energy K, the potential energy P and the rate of energy dissipation D of this coupled system are expressed as

$$\left.\begin{gathered} K_\mathrm{s} = \tfrac{1}{2}\dot{\phi}^2, \quad K_\mathrm{w} = \tfrac{1}{2}\rho(\dot{x}_{G_\mathrm{w}}^2 + \dot{y}_{G_\mathrm{w}}^2), \\ P_\mathrm{s} = -(1+\rho)\sigma^2 y_{B_\mathrm{s}}, \quad P_\mathrm{w} = \rho\sigma^2 y_{G_\mathrm{w}}, \quad P_\mathrm{f} = -\phi\{A_0 + A_1\sin(\Omega t + \psi)\}, \\ D = \tfrac{1}{2}\nu_\mathrm{s}\dot{\phi}^2 + \tfrac{1}{2}\nu_\mathrm{w}\dot{\chi}^2, \end{gathered}\right\} \quad (3.1)$$

where mass and length are normalized by the mass of the ship M and the radius of gyration κ, x and y denote the horizontal and vertical coordinates, with the origin set at the centre of gravity of the ship G_s as shown in figure 8. The subscripts s, w and f denote the ship, the flooded water and the wave-forcing moment, respectively, $\rho{=}m/M$, where m is the mass of the flooded water, $\sigma = \sqrt{g/\kappa}$, where g is the gravitational acceleration, $\boldsymbol{x}_{G_\mathrm{w}} = (x_{G_\mathrm{w}}, y_{G_\mathrm{w}})$ is the location of the centre of gravity G_w of the flooded water, $\boldsymbol{x}_{B_\mathrm{s}} = (x_{B_\mathrm{s}}, y_{B_\mathrm{s}})$ is the location of the centre of buoyancy B_s of the ship, $A_0 + A_1\sin(\Omega t + \psi)$ is the wave-forcing moment, and ν the damping coefficient. Note that the time t is not normalized.

The dissipation in this system is mainly due to the viscous effects. The roll motion of the ship is also subjected to the wave-making damping. The coefficients ν_s and ν_w can be experimentally estimated by free damping tests in still water, with and without flooded water inside a ship.

Although we do not aim at quantitative comparison between this mathematical model and the experimental results, it is important to see the practical range of values of the amplitude of the wave-exciting moment A_1 and the constant heel moment A_0. The wave-exciting moment is often expressed as $\tilde{A}_1 = Mg\overline{GM}\zeta\Theta_\mathrm{w}$, where $\overline{GM}$ denotes the metacentric height above the centre of gravity of the ship, ζ (*ca.* 0.7–0.8)

the effective wave slope, and Θ_{w} the wave slope. Thus $A_1 = \tilde{A}_1/(M\kappa^2)$ roughly ranges from 0 to 1.5 s^{-2} in the experimental scale, and from 0 to 0.05 s^{-2} in a real ship scale. The constant heel moment A_0 is due to the steady loading such as the viscous resistance, the wave drift force, the wind force, shift of cargo and vehicles, and so on. Since it is hard to experimentally estimate all of them, the value of A_0 in the numerical calculation in § 4 was set so that the constant heel angle ϕ_0 was increased by 0–5°.

Substitution of $K = K_{\mathrm{s}} + K_{\mathrm{w}}$, $P = P_{\mathrm{s}} + P_{\mathrm{w}} + P_{\mathrm{f}}$ and D into Lagrange's equations of motion with the Lagrangian $L = K - P$ produces a mathematical model for the coupled motion. We can geometrically determine $y_{B_{\mathrm{s}}}(\phi)$ and $\boldsymbol{x}_{G_{\mathrm{w}}}(\phi, \chi)$ in (3.1) (Murashige & Aihara 1998*b*). Here, $\boldsymbol{x}_{G_{\mathrm{w}}}(\phi, \chi)$ can be written in the form

$$\boldsymbol{x}_{G_{\mathrm{w}}} = \begin{pmatrix} x_G(\phi,\chi) \\ y_G(\phi,\chi) \end{pmatrix} = \begin{pmatrix} \cos\phi & \sin\phi \\ -\sin\phi & \cos\phi \end{pmatrix} \begin{pmatrix} \xi_G(\chi) \\ \eta_G(\chi) \end{pmatrix}. \tag{3.2}$$

The kinetic energy of flooded water K_{w} can be expressed as

$$K_{\mathrm{w}} = \tfrac{1}{2}\rho\{q_1(\chi)\dot{\phi}^2 + 2q_2(\chi)\dot{\phi}\dot{\chi} + q_3(\chi)\dot{\chi}^2\}, \tag{3.3}$$

where q_1, q_2 and q_3 are given by

$$\left.\begin{aligned} q_1(\chi) &= {\xi_G}^2 + {\eta_G}^2, \\ q_2(\chi) &= \frac{\partial \xi_G}{\partial \chi} \cdot \eta_G - \xi_G \cdot \frac{\partial \eta_G}{\partial \chi}, \\ q_3(\chi) &= \left(\frac{\partial \xi_G}{\partial \chi}\right)^2 + \left(\frac{\partial \eta_G}{\partial \chi}\right)^2. \end{aligned}\right\} \tag{3.4}$$

The equations of motion can be written in the form

$$\boldsymbol{M}_0\ddot{\boldsymbol{\Phi}}_0 + \boldsymbol{N}_0\dot{\boldsymbol{\Phi}}_0 + \boldsymbol{h}_0 + \boldsymbol{r}_0 = \boldsymbol{f}, \tag{3.5}$$

where $\boldsymbol{\Phi}_0 = (\phi, \chi)^{\mathrm{T}}$, $^{\mathrm{T}}$ denotes the transpose and

$$\left.\begin{aligned} \boldsymbol{M}_0 &= \begin{pmatrix} 1+\rho q_1 & \rho q_2 \\ \rho q_2 & \rho q_3 \end{pmatrix}, \\ \boldsymbol{N}_0 &= \begin{pmatrix} \nu_{\mathrm{s}} & 0 \\ 0 & \nu_{\mathrm{w}} \end{pmatrix}, \\ \boldsymbol{h}_0 &= \begin{pmatrix} \rho\left(\dfrac{\partial q_1}{\partial \chi}\dot{\phi}\dot{\chi} + \dfrac{\partial q_2}{\partial \chi}\dot{\chi}^2\right) \\ \tfrac{1}{2}\rho\left(-\dfrac{\partial q_1}{\partial \chi}\dot{\phi}^2 + \dfrac{\partial q_3}{\partial \chi}\dot{\chi}^2\right) \end{pmatrix}, \\ \boldsymbol{r}_0 &= \sigma^2 \begin{pmatrix} -(1+\rho)\dfrac{\partial y_B}{\partial \phi} - \rho(\xi_G\cos\phi + \eta_G\sin\phi) \\ \rho\left(-\dfrac{\partial \xi_G}{\partial \chi}\sin\phi + \dfrac{\partial \eta_G}{\partial \chi}\cos\phi\right) \end{pmatrix}, \\ \boldsymbol{f} &= \begin{pmatrix} A_0 + A_1\sin(\Omega t + \psi) \\ 0 \end{pmatrix}. \end{aligned}\right\} \tag{3.6}$$

In addition, equation (3.5) can be rewritten in the form

$$\frac{\mathrm{d}\boldsymbol{u}}{\mathrm{d}t} = \boldsymbol{F}(t, \boldsymbol{u}), \tag{3.7}$$

where $\boldsymbol{u} = (\phi, \chi, \dot{\phi}, \dot{\chi})^{\mathrm{T}}$ and

$$\boldsymbol{F} = \begin{pmatrix} \dot{\boldsymbol{\Phi}}_0 \\ \boldsymbol{M}_0{}^{-1}(-\boldsymbol{N}_0\dot{\boldsymbol{\Phi}}_0 - \boldsymbol{h}_0 - \boldsymbol{r}_0 + \boldsymbol{f}) \end{pmatrix}. \tag{3.8}$$

(*b*) *Characteristics of this nonlinearly coupled system*

The vector field $\boldsymbol{F}$ in (3.7) has a complicated form and is piecewise nonlinear with respect to $\boldsymbol{u}$ (Murashige *et al.* 1997). The piecewise nonlinearity is not a physically required property, but an artificially introduced one on the assumptions of this model as follows. $\boldsymbol{x}_{B_{\mathrm{s}}}$ corresponds to the centre of the cross-section of the ship under the still water surface, and, similarly, $\boldsymbol{x}_{G_{\mathrm{w}}}$ corresponds to the centre of the cross-section of flooded water. Each sectional shape changes from a trapezoid to a triangle at $\phi = \phi^* = \tan^{-1} 2d_{\mathrm{s}}/b_{\mathrm{s}}$ and $\chi = \chi^* = \tan^{-1} 2d_{\mathrm{w}}/b_{\mathrm{w}}$, respectively (see figure 8). Although the vector $\boldsymbol{F}$ in (3.7) is continuous with respect to ϕ and χ, the Jacobian matrix $\partial\boldsymbol{F}/\partial\boldsymbol{u}$ and higher-order partial derivatives are discontinuous at $\phi = \phi^*$ and $\chi = \chi^*$. This discontinuity can cause some troubles in numerically calculating bifurcation sets of this model. In order to avoid these troubles, we try to derive a simplified model with a smooth vector field, but without losing essential properties of the original model.

(i) *The potential energy P*

The bistable condition characterizes the potential energy of this system, as we previously indicated (Murashige & Aihara 1998*b*). Namely, there are three statically equilibrium positions of which two are stable at $\phi = \pm\phi_{\mathrm{e}}$ and one is unstable at the horizontal position $\phi = 0$. The simplest form for this condition may be given by

$$\frac{\partial P_0}{\partial \phi} \propto \phi(\phi^2 - {\phi_{\mathrm{e}}}^2) \quad \text{at } \phi = \chi, \tag{3.9}$$

where $P_0 = P_{\mathrm{s}} + P_{\mathrm{w}}$ (see (3.1)). In addition, we should note that, at a statically balanced position, the surface of flooded water is horizontal ($\chi = \phi$). This condition can be expressed as

$$\frac{\partial P_0}{\partial \chi} \propto \phi - \chi. \tag{3.10}$$

For the sake of convenience, hereafter we use θ for the inclination of the surface of flooded water in the spatially fixed coordinate system, instead of χ in the body-fixed coordinate system (see figure 8). One of the possible forms of the potential energy $P(\phi, \theta)$, which satisfies the above two conditions, is

$$P_1(\phi, \theta) = \sigma^2\{(\alpha_0 + \alpha_2\phi^2)\theta^2 + \gamma_2\phi^2 + \gamma_4\phi^4\}, \tag{3.11}$$

where α_0, α_2, γ_2 and γ_4 are constant. Figure 9 compares the contour plots of P_0 and P_1 in the (ϕ, χ)-plane.

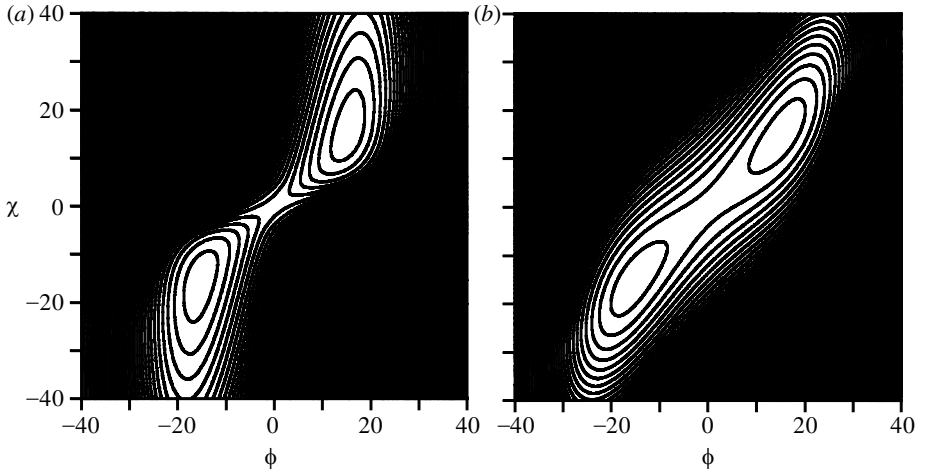

Figure 9. Comparison of the contour plots of the potential energy P_0 and P_1 in the (ϕ, χ)-plane. $P_0 = P_s + P_w$ (see (3.1)). Unit: degree. Step value of contour: 0.05.

It should be noted that the potential energy of this model does not express extremely large amplitude motion which may lead to capsizing. This is because we only consider nonlinear responses found in the experiments where the wave height was relatively moderate and capsizing was not found (Murashige & Aihara 1998*b*).

(ii) *The kinetic energy K*

The kinetic energy of flooded water K_w can be rewritten, using θ, in the form

$$K_w(\phi, \theta) = \tfrac{1}{2}\rho\{(q_1 + 2q_2 + q_3)\dot{\phi}^2 + 2(q_2 + q_3)\dot{\phi}\dot{\theta} + q_3\dot{\theta}^2\}, \tag{3.12}$$

and the main properties of this energy can be approximated by

$$K_w(\phi, \theta) \simeq K_1(\phi, \theta) = \tfrac{1}{2}\rho q_0(\phi, \theta)(\dot{\phi}^2 + \dot{\theta}^2). \tag{3.13}$$

Here, $q_0(\phi, \theta)$ is given by

$$q_0(\phi, \theta) = \frac{c_2}{1 + c_1(\phi + \theta)^2}, \tag{3.14}$$

where c_1 and c_2 are constant.

(iii) *A new model for motion of a flooded ship in waves*

Substitution of the potential energy $P = P_1$ and the kinetic energy $K = K_s + K_1$ into Lagrange's equations of motion yields

$$\boldsymbol{M}_1\ddot{\boldsymbol{\Phi}}_1 + \boldsymbol{N}_1\dot{\boldsymbol{\Phi}}_1 + \boldsymbol{h}_1 + \boldsymbol{r}_1 = \boldsymbol{f}, \tag{3.15}$$

where $\boldsymbol{\Phi}_1 = (\phi, \theta)^{\mathrm{T}}$ and

$$\left.\begin{aligned} \boldsymbol{M}_1 &= \begin{pmatrix} 1+\rho q_0 & \rho q_0 \\ \rho q_0 & \rho q_0 \end{pmatrix}, \\ \boldsymbol{h}_1 &= \tfrac{1}{2}\rho \frac{\partial q_0}{\partial \phi}(\dot{\phi}+\dot{\theta})^2 \begin{pmatrix} 1 \\ 1 \end{pmatrix}, \\ \boldsymbol{N}_1 &= \begin{pmatrix} \nu_\phi & 0 \\ 0 & \nu_\theta \end{pmatrix}, \\ \boldsymbol{r}_1 &= \sigma^2 \begin{pmatrix} 2\alpha_2\phi\theta^2 + 2\gamma_2\phi + 4\gamma_4\phi^3 \\ 2(\alpha_0+\alpha_2\phi^2)\theta \end{pmatrix}. \end{aligned}\right\} \tag{3.16}$$

Here it should be noted that the damping moments are assumed to vary linearly with $\dot{\phi}$ and $\dot{\theta}$ with the coefficients ν_ϕ and ν_θ, respectively.

This model can be classified into a type of coupled Duffing's equations. A representative example of a coupled mechanical system which produces chaotic behaviour is a double pendulum. Also, there are some similar coupled systems, such as roll and heave of a ship in waves (Thompson & de Souza 1996). In comparison with these other coupled systems, this model is unique in the sense that it includes both the bistable restoring term and the nonlinear coefficient matrix $\boldsymbol{M}_1$.

4. Bifurcation analyses

(*a*) *Bifurcation diagrams of periodic responses*

We can obtain bifurcation sets of periodic solutions of the model (3.15) using the periodic condition, the bifurcation condition and Newton's method (Kawakami 1984). Figure 10*a* shows the two-parameter bifurcation diagrams of the period-1 and period-2 solutions in the (Ω, A_1)-plane when $\rho = 0.1$, $A_0 = 0$, $\nu_\phi = 0.05$ and $\nu_\theta = 0.05$. In this condition, the constant heel angle ϕ_0 in a still water is equal to 15.4°. Here, the 'period-N' solution denotes a solution of which the period is $2N\pi/\Omega$. The other parameter values are closely set to those of the experiments using the box-shaped model (Murashige & Aihara 1998*b*). Figures 10–14 are shown in the experimental scale, and the frequency range corresponds to that of waves in real sea. Figure 10*b* shows an enlarged diagram of figure 10*a* near $\Omega = 5.0$. This diagram is similar to the result of the original model (3.5) (see fig. 5 in Murashige *et al*. 1999). In particular, the period-1 and -2 solutions coexist in a region $(\Omega, A_1) = (4.0\text{–}5.0, 0.05\text{–}0.4)$ surrounded by the bifurcation curves G^2 (saddle-node), I^2 (period-doubling) and H^2 (Neimark–Sacker). The experiments using the ferry model (Murashige & Aihara 1998*b*) were performed in this region and we found coexistence of the small-amplitude period-1 and the large-amplitude period-2 responses. This result suggests that the simplified model of (3.15) keeps the essential features of the experimental results and the original model.

Figure 11*a*, *b* shows the bifurcation diagrams for $A_0 = 0.5$ and 1.0, respectively, with the values of the other parameters as in figure 10. Note that the frequency range in figure 11 is not the same as in figure 10. In these conditions, the constant heel angles ϕ_0 are equal to 18.5° for $A_0 = 0.5$, and 20.6° for $A_0 = 1.0$, respectively, when the ship is set in a statically balanced position in a still water, namely A_1 being set to zero. This bias term A_0 is related to the symmetry of this system

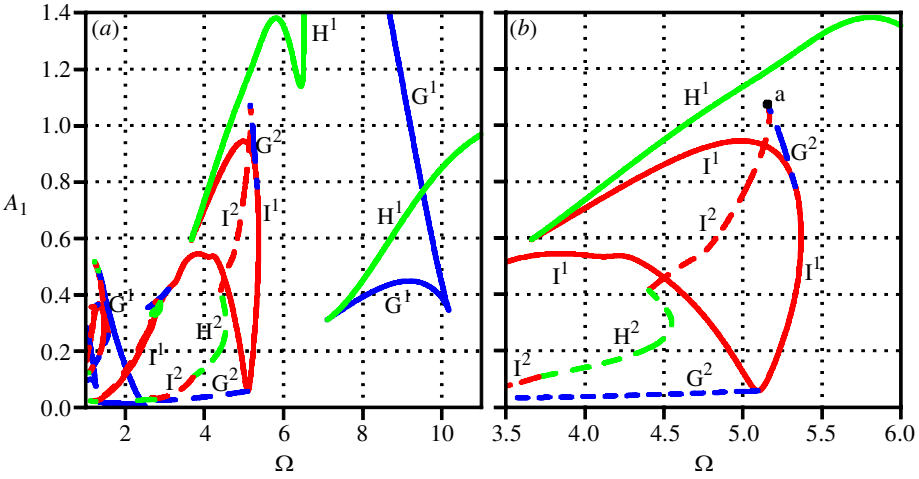

Figure 10. Two-parameter bifurcation diagrams in the (Ω, A_1)-plane ($\rho = 0.1$, $A_0 = 0$, $\nu_\phi = 0.05$ and $\nu_\theta = 0.05$). The other parameter values are closely set to the experiments using the box-shaped model. The wave-exciting moment A_1 s^{-2} and the wave frequency Ω rad s^{-1} are represented in the experimental scale. The point 'a' in (*b*) denotes the codimension-two bifurcation point at which the saddle-node and the period-doubling bifurcations occur (see figure 14*a*). Solid line: bifurcation curves of the period-1 solution. Dashed line: bifurcation curves of the period-2 solution. G^N (blue line): the saddle-node bifurcation. I^N (red line): the period-doubling bifurcation. H^N (green line): the Neimark–Sacker bifurcation. ^{N}: the period N solution.

(Murashige *et al.* 1999). Bifurcation structures in figures 10 and 11 are similar, but the corresponding frequencies are different and the bifurcation curves move to the right side in the (Ω, A_1)-plane with increasing A_0. This is because the resonance frequencies of the coupled system subjected to the periodic wave-forcing increase with A_0 (Murashige *et al.* 1999). Near the resonance frequencies, the bifurcation curves come down to the small value of A_1, for example, $\Omega \simeq 1.5$, 3.2 and 6.5 in figure 11*a*, and $\Omega \simeq 1.9$, 3.8 and 7.7 in figure 11*b*. In particular, we consider the regions $(\Omega, A_1) = (2.0\text{–}3.5, 0.0\text{–}0.6)$ in figure 11*a* and $(\Omega, A_1) = (2.5\text{–}4.0, 0.0\text{–}0.8)$ in figure 11*b* to be important from the viewpoint of not only mathematical interests, but also engineering applications. This is because complicated bifurcation phenomena occur even at small values of A_1, and some of the chaotic solutions in these regions are similar to the measured chaotic responses in the experiments, as shown later in figure 13. The chaotic solutions are found in the regions where A_1 is larger than that of the bifurcation curves I^1 and H^1 in figure 11*a* and H^1 in figure 11*b*. It should be noted that chaotic responses exist in wide regions of the parameter space, even if the wave-exciting moment is not large, as found in the experiments. Thus it may be possible to catch the mechanism of generation of complex nonlinear responses observed in the experiments by further detailed bifurcation analyses using this mathematical model. In the next section, we investigate one-parameter bifurcation for $A_1 = 0.0\text{–}0.8$ and Ω fixed to 3.5 in figure 11*b*.

(*b*) *Generation of chaotic responses*

Figure 12 represents the one-parameter bifurcation diagram with a change in the amplitude of the wave-exciting moment A_1 for $(\Omega, A_1) = (3.5, 0.0\text{–}0.8)$ in figure 11*b*.

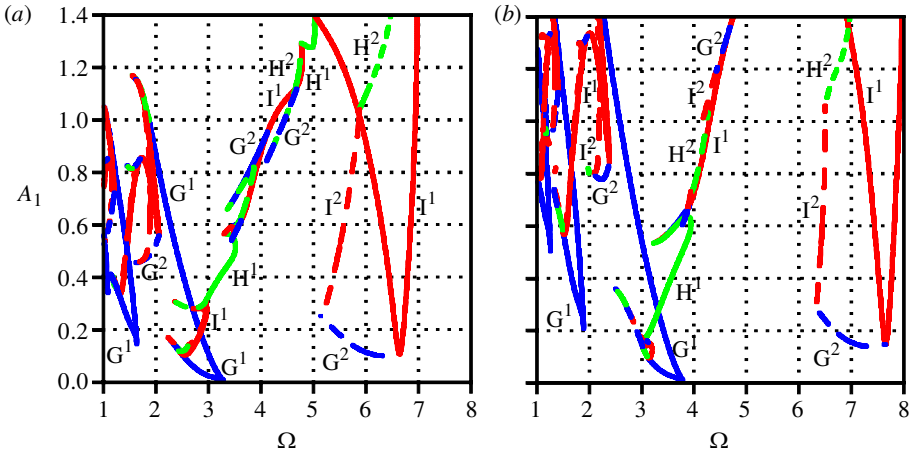

Figure 11. Two-parameter bifurcation diagrams in the (Ω, A_1)-plane ($\rho = 0.1$, $\nu_\phi = 0.05$ and $\nu_\theta = 0.05$). (*a*) $A_0 = 0.5$. (*b*) $A_0 = 1.0$. (See caption to figure 10.)

Figure 12*a* shows the variation of the stroboscopic plots of the roll angle $\phi(t_0 + k2\pi/\Omega)$, $k = 0, 1, 2, \ldots, 30$. The corresponding Lyapunov exponents are shown in figure 12*b*. In figure 12*a*, *b*, A_1 is increased from 0 to 0.8, and there are mainly two bifurcation points at $A_1 = 0.14$ and 0.37. These two figure parts indicate that chaotic responses with the positive Lyapunov exponent can be found for $A_1 > 0.37$. Figure 12*c* shows the variation of ϕ at the fixed point of the period-1 solution and its stability with A_1. The stable and unstable fixed points are connected by the solid and dotted lines, respectively. The fixed point and its stability can be obtained using the Poincaré mapping $\boldsymbol{T}$, defined by

$$\boldsymbol{T} : \boldsymbol{u}(t = t_0) = \boldsymbol{u}_0 \mapsto \boldsymbol{u}(t = t_0 + 2\pi/\Omega). \tag{4.1}$$

The period-N solutions satisfy the fixed-point condition $\boldsymbol{T}^N(\boldsymbol{u}_0) = \boldsymbol{u}_0$, with $\boldsymbol{T}^k(\boldsymbol{u}_0) \neq \boldsymbol{u}_0$ for $k = 1, 2, \ldots, N-1$. The eigenvalues of $\partial \boldsymbol{T}^N / \boldsymbol{u}_0$ determine the stability of the periodic solutions and topological properties including the type of bifurcation. Figure 12*c* shows the hysteresis phenomenon for $0.0 < A_1 < 0.2$, where the two stable period-1 solutions coexist between the two saddle-node (fold) bifurcation points G^1 at $A_1 = 0.03$ and 0.14. Thus, when A_1 is decreased from 0.2 to 0, the period-1 solution disappears at $A_1 = 0.03$. The period-1 solution for $A_1 > 0.3$ is destabilized at $A_1 \simeq 0.37$ and transits to a quasi-periodic solution because of the Neimark–Sacker bifurcation. These results correspond to the bifurcation along $(\Omega, A_1) = (3.5, 0.0\text{–}0.8)$ in figure 11*b*. It should be noted that if quasi-periodic solutions do exist, then they seem to exist in the very limited regions of A_1, and that the chaotic solution is found in the wide regions.

Figure 13 displays an attractor of a chaotic solution, which corresponds to $A_1 = 0.6$ in figure 12 ($\rho = 0.1$ and $A_0 = 1.0$). This attractor is reconstructed using the delay coordinates $(\phi(t), \phi(t + \tau), \phi(t + 2\tau))$ with $\tau = \frac{1}{4}(2\pi/\Omega)$. The geometrical structure of this attractor is similar to that of the experimental results in figure 2.

The next step is to investigate the mechanism of these nonlinear phenomena, including the generation of chaos. The dynamical structure of a low-dimensional system such as the Duffing equation has been considered in detail. For example,

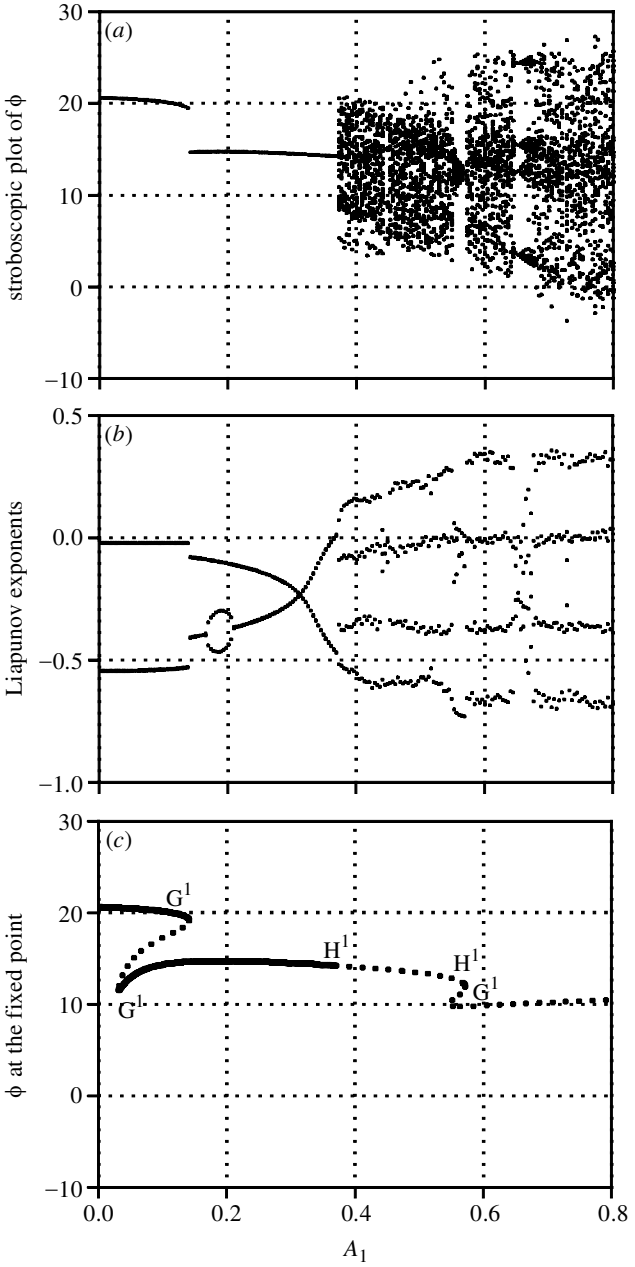

Figure 12. One-parameter bifurcation diagram with change of A_1 ($\rho = 0.1$, $A_0 = 1.0$, $\Omega = 3.5\,\mathrm{rad\,s^{-1}}$, $\nu_\phi = 0.05$ and $\nu_\theta = 0.05$) (ϕ measured in degrees). (*a*) Stroboscopic plots of the roll angle $\phi(t_0 + k2\pi/\Omega)$, $k = 0, 1, 2, \ldots, 30$. (*b*) Lyapunov exponents. (*c*) The roll angle ϕ at the fixed point of the period-1 solution (solid line, stable; dotted line, unstable; see caption to figure 10).

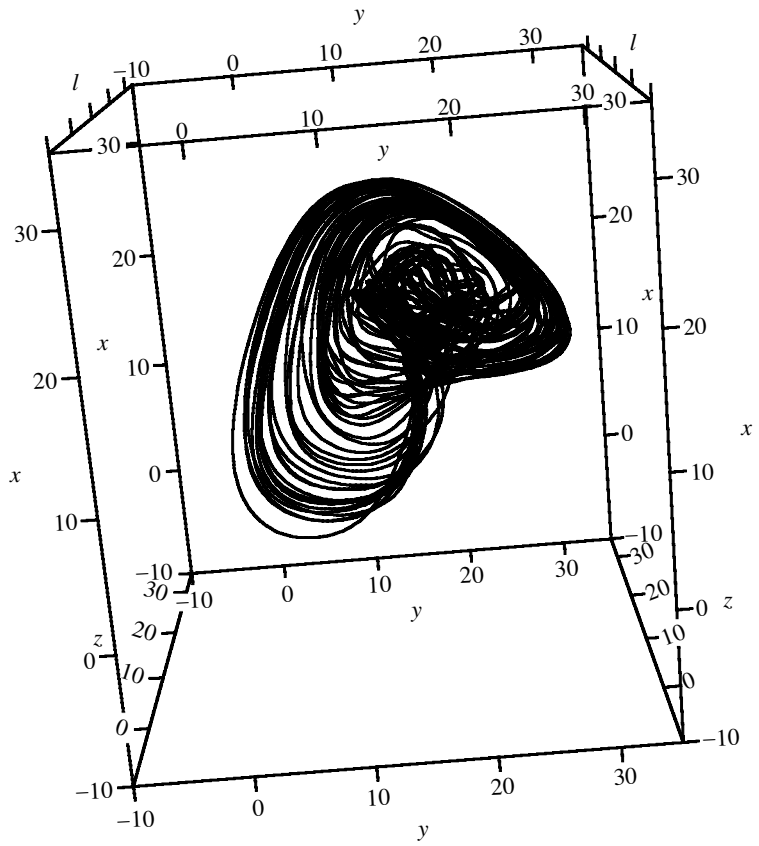

Figure 13. An attractor of a chaotic solution of the mathematical model ($A_0 = 1.0$, $A_1 = 0.6$, $\Omega = 3.5$, $\nu_\phi = 0.05$ and $\nu_\theta = 0.05$). This attractor is reconstructed using the delay coordinates $(x, y, z) = (\phi(t), \phi(t+\tau), \phi(t+2\tau))$, where $\tau = \frac{1}{4}(2\pi/\Omega)$. Unit: degree.

Thompson (1989, 1997) thoroughly examined it for roll motion of a ship in waves. On the other hand, a coupled system such as the present model can produce more complicated phenomena than a single system. It is well known that the single Duffing system cannot give the Neimark–Sacker bifurcation, which yields quasi-periodic solutions, but the coupled Duffing systems can (Kawakami 1984; Thompson & de Souza 1996). Although the intricate dynamical structure of the coupled system has not been fully elucidated, bifurcation analyses may help us understand it in a systematic way. For periodic solutions in this type of system, there are three general types of the codimension-one bifurcation, namely, the saddle-node, the period-doubling and the Neimark–Sacker bifurcation. In such a high-dimensional system, two of the codimension-one bifurcations can easily occur at the same parameter values, just like the point 'a' in figure 10*b*. This codimension-two bifurcation occurs not in a wide region, but at some points in the parameter space. Yoshinaga & Kawakami (1989) showed some numerical solutions which imply a complicated structure of solutions and a new type of route from periodic solutions to chaos near the codimension-two bifurcation point, using a mathematical model for a coupled electrical circuit. Figure 14*a* shows the bifurcation curves of the period-2 and -4 solutions near the point

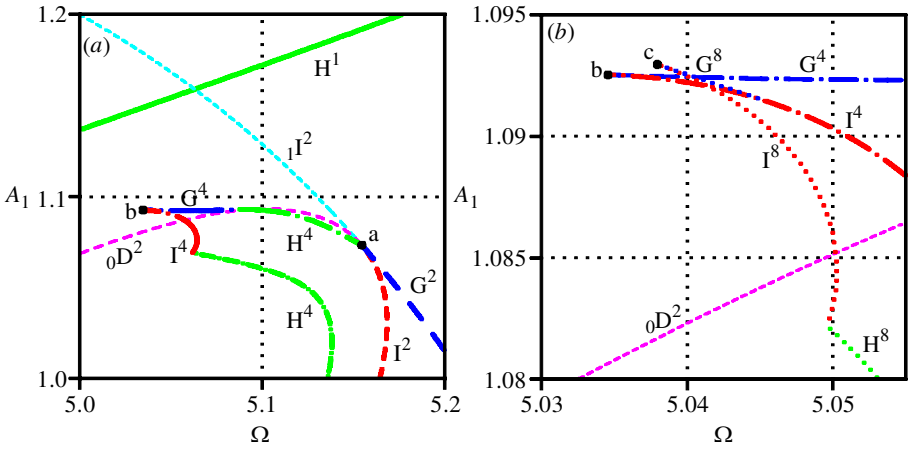

Figure 14. Two-parameter bifurcation diagrams near the codimension-two bifurcation points. Dashed line: bifurcation curves of the period-2 solutions. Dot–dashed line: bifurcation curves of the period-4 solutions. Dotted line: bifurcation curves of the period-8 solutions. ${}_0\mathrm{D}^2$ (pink): $\mu_1 > 1$, $\mu_2 = -1$, $|\mu_{3,4}| < 1$. ${}_1\mathrm{I}^2$ (cyan): $\mu_1 < -1$, $\mu_2 = 1$, $|\mu_{3,4}| < 1$. The μ_i are the eigenvalues of $\partial \boldsymbol{T}^2/\partial \boldsymbol{u}_0$. The points 'a', 'b' and 'c' are the codimension-two bifurcation points. (See caption to figure 10.)

'a' in figure 10*b*, at which both the saddle-node and the period-doubling bifurcations simultaneously occur. This figure includes the bifurcation curves ${}_0\mathrm{D}^2$ (pink) and ${}_1\mathrm{I}^2$ (cyan) of the unstable period-2 solution. We can see another codimension-two bifurcation point 'b' of the period-4 solution. Figure 14*b* shows bifurcation of the period-4 and -8 solutions near the point 'b' in figure 14*a*. It should be noted that a chain of the codimension-two bifurcation points of the period-2, -4, and -8 solutions is found in figure 14. With this chain, the accumulation of the saddle-node, the period-doubling and the Neimark–Sacker bifurcations can occur. This route to chaos is not found in a single system of the Duffing equation. The wave-exciting moment A_1 in figure 14 is larger than that in figure 13, but there are some other codimension-two bifurcation points in figure 11 at the smaller values of A_1. Thus this type of bifurcation may be related to the generation of chaos in this coupled system. Further bifurcation analyses are required for full elucidation of this intricate structure, which we could not catch in previous experimental work.

5. Conclusions

We have considered the nonlinear roll motion of a flooded ship in regular waves, by nonlinear time-series analyses of the experimental results and bifurcation analyses of the mathematical model.

In previous work (Murashige & Aihara 1998*b*), the experiments demonstrated that a flooded ship can exhibit complicated irregular roll motion in regular waves. The present results of the fractal dimension and the Lyapunov exponents of the experimental data indicate that they have chaotic characteristics. In addition, the RBF network obtained directly from the data reproduces the geometrical structure of the reconstructed attractor and provides good short-term prediction on the dynamical motion.

We have also simplified the mathematical model used in previous work (Murashige *et al*. 1999), in order to avoid some troubles for bifurcation analyses in the original model. This model can be classified into a coupled system of two Duffing's equations with the bistable restoring term and the nonlinear inertia coefficients. We obtained some bifurcation diagrams using the simplified model, and found that it can produce chaotic responses in the wide regions of the parameter space even if the wave-exciting moment is not large. Furthermore, the attractor of the chaotic solution is geometrically similar to that of the measured chaotic motion in the experiments. The results suggest that further bifurcation analyses using this model may lead us to fully understand the complex nonlinear responses of a flooded ship in waves.

The authors thank the Ship Research Institute, Ministry of Transport, Japan, for help with experiments, Dr Motomasa Komuro of Teikyo University of Science and Technology, Dr Hiroshi Kawakami, Dr Tetsuya Yoshinaga and Dr Tetsushi Ueta of the University of Tokushima for enlightening discussions on bifurcation, and two anonymous reviewers for their constructive comments.

References

Abarbanel, H. D. I. 1996 *Analysis of observed chaotic data*. Springer.

Casdagli, M. 1989 Nonlinear prediction of chaotic time series. *Physica* D **35**, 335–356.

Dillingham, J. 1981 Motion studies of a vessel with water on deck. *Marine Tech.* **18**, 38–50.

Eckmann, J. P. & Ruelle, D. 1985 Ergodic theory of chaos and strange attractors. *Rev. Mod. Phys.* **57**, 617–656.

Falzarano, J. M., Shaw, S. W. & Troesch, A. W. 1992 Application of global methods for analyzing dynamical systems to ship rolling motion and capsizing. *Int. J. Bifurcation Chaos* **2**, 101–115.

Farmer, J. D. & Sidorowich, J. J. 1987 Predicting chaotic time series. *Phys. Rev. Lett.* **59**, 845–858.

Grassberger, P. & Procaccia, I. 1983*a* Measuring strangeness of strange attractors. *Physica* D **9**, 189–208.

Grassberger, P. & Procaccia, I. 1983*b* Characterization of strange attractors. *Phys. Rev. Lett.* **50**, 346–349.

Judd, K. 1992 An improved estimator of dimension and some comments on providing confidence intervals. *Physica* D **56**, 216–228.

Judd, K. 1994 Estimating dimension from small samples. *Physica* D **71**, 421–429.

Kan, M. & Taguchi, H. 1990 Capsizing of a ship in quatering seas. Part 2. Chaos and fractal in capsizing phenomenon. *J. Soc. Naval Architects Japan* **168**, 211–220.

Kantz, H. & Schreiber, T. 1997 *Nonlinear time series analysis*. Cambridge University Press.

Kawakami, H. 1984 Bifurcation of periodic responses in forced dynamic nonlinear circuits: computation of bifurcation values of the system parameters. *IEEE Trans. Circuits Systems* **31**, 248–260.

MacMaster, A. G. & Thompson, J. M. T. 1994 Wave tank testing and the capsizability of hulls. *Proc. R. Soc. Lond.* A **446**, 217–232.

Miles, J. W. & Henderson, D. 1990 Parametrically forced surface waves. *A. Rev. Fluid Mech.* **22**, 143–165.

Moon, F. C. 1992 *Chaotic and fractal dynamics*. Wiley.

Murashige, S. & Aihara, K. 1998*a* Coexistence of periodic roll motion and chaotic one in a forced flooded ship. *Int. J. Bifurcation Chaos* **8**, 619–626.

Murashige, S. & Aihara, K. 1998*b* Experimental study on chaotic motion of a flooded ship in waves. *Proc. R. Soc. Lond.* A **454**, 2537–2553.

Murashige, S., Komuro, M. & Aihara, K. 1997 Non-smooth characteristics and bifurcation of a mathematical model for non-linear motion of a flooded ship in waves. In *Proc. 1997 Int. Symp. on Nonlinear Theory and its Applications (NOLTA '97)*, vol. 1, pp. 497–500.

Murashige, S., Komuro, M. & Aihara, K. 1999 Bifurcation and resonance of a mathematical model for non-linear motion of a flooded ship in waves. *J. Sound Vib.* **220**, 155–170.

Nayfeh, A. H. 1988 On the undesirable roll characteristics of ships in regular seas. *J. Ship Res.* **32**, 92–100.

Nayfeh, A. H. & Mook, D. T. 1979 *Nonlinear oscillations*. Wiley.

Nayfeh, A. H., Mook, D. T. & Marshall, L. R. 1973 Nonlinear coupling of pitch and roll modes in ship motions. *J. Hydronautics* **7**, 145–152.

Ott, E., Sauer, T. & Yorke, J. A. 1994 *Coping with chaos*. Wiley.

Parker, T. S. & Chua, L. O. 1989 *Practical numerical algorithms for chaotic systems*. Springer.

Paulling, J. R. & Rosenberg, R. M. 1959 On unstable ship motions resulting from nonlinear coupling. *J. Ship Res.* **3**, 36–46.

Rainey, R. C. T. & Thompson, J. M. T. 1991 The transient capsize diagram—a new method of quantifying stability in waves. *J. Ship Res.* **35**, 58–62.

Ruelle, D. 1990 Deterministic chaos: the science and the fiction. *Proc. R. Soc. Lond.* A **427**, 241–248.

Sano, M. & Sawada, Y. 1985 Measurement of the Lyapunov spectrum from a chaotic time series. *Phys. Rev. Lett.* **55**, 1082–1085.

Sauer, T., Yorke J. A. & Casdagli, M. 1991 Embedology. *J. Statist. Phys.* **65**, 579–616.

Shimada, I. & Nagashima, T. 1979 A numerical approach to ergodic problem of dissipative dynamical systems. *Prog. Theoret. Phys.* **61**, 1605–1616.

Skarda, C. A. & Freeman, W. J. 1987 How brains make chaos in order to make sense of the world. *Behav. Brain Sci.* **10**, 161–195.

Smith, L. A. 1993 Does a meeting in Santa Fe imply chaos? In *Time series prediction: forecasting the future and understanding the past* (ed. A. S. Weigend & N. A. Gershenfeld), pp. 323–343. Addison-Wesley.

Soliman, M. S. & Thompson, J. M. T. 1991 Transient and steady state analysis of capsize phenomena. *Appl. Ocean Res.* **13**, 82–92.

Sugihara, G. & May, R. M. 1990 Nonlinear forecasting as a way of distinguishing chaos from measurement error in time series. *Nature* **344**, 734–741.

Suzuki, M., Judd, K., Aihara, K. & Kotani, M. 1993 Approximation of the logistic mapping with radial basis function networks. *IEICE* A **8**, 1177–1184.

Takens, F. 1981 Detecting strange attractors in turbulence. In *Dynamical systems and turbulence* (ed. D. A. Rand & B. S. Young). Lecture Notes in Mathematics, vol. 898, pp. 366–381. Springer.

Thompson, J. M. T. 1989 Chaotic phenomena triggering the escape from a potential well. *Proc. R. Soc. Lond.* A **421**, 195–225.

Thompson, J. M. T. 1997 Designing against capsize in beam seas: Recent advances and new insights. *Appl. Mech. Rev.* **50**, 307–325.

Thompson, J. M. T. & de Souza, J. R. 1996 Suppression of escape by resonant modal interactions: in shell vibration and heave–roll capsize. *Proc. R. Soc. Lond.* A **452**, 2527–2550.

Thompson, J. M. T., Rainey, R. C. T. & Soliman, M. S. 1992 Mechanics of ship capsize under direct and parametric wave excitation. *Phil. Trans. R. Soc. Lond.* A **338**, 471–490.

Virgin, L. N. 1987 The nonlinear rolling response of a vessel including chaotic motions leading to capsize in regular seas. *Appl. Ocean Res.* **9**, 89–95.

Wright, J. H. G. & Marshfield, W. B. 1980 Ship roll response and capsize behaviour in beam seas. *Trans. RINA* **122**, 129–148.

Yoshinaga, T. & Kawakami, H. 1989 Codimension two bifurcation in nonlinear circuits with periodically forcing term. *Trans. IEICE Japan* A **72**, 1821–1828.